Effect of mass transfer on the oxygen reduction reaction catalyzed by platinum dendrimer encapsulated nanoparticles

Ioana Dumitrescu and Richard M. Crooks[1]

Department of Chemistry and Biochemistry, Center for Electrochemistry, and the Center for Nano- and Molecular Science and Technology, University of Texas at Austin, 1 University Station, A5300, Austin, TX 78712-0165

Edited by Royce W. Murray, University of North Carolina, Chapel Hill, NC, and approved April 24, 2012 (received for review January 25, 2012)

Here we report on the effect of the mass transfer rate (k_t) on the oxygen reduction reaction (ORR) catalyzed by Pt dendrimer-encapsulated nanoparticles (DENs) comprised of 147 and 55 atoms (Pt_{147} and Pt_{55}). The experiments were carried out using a dual-electrode microelectrochemical device, which enables the study of the ORR under high k_t conditions with simultaneous detection of H_2O_2. At low k_t (0.02 to 0.12 cm s^{-1}) the effective number of electrons involved in ORR, n_{eff}, is 3.7 for Pt_{147} and 3.4 for Pt_{55}. As k_t is increased, the mass-transfer-limited current for the ORR becomes significantly lower than the value predicted by the Levich equation for a 4-electron process regardless of catalyst size. However, the percentage of H_2O_2 detected remains constant, such that n_{eff} barely changes over the entire k_t range explored (0.02 cm s^{-1}). This suggests that mass transfer does not affect n_{eff}, which has implications for the mechanism of the ORR on Pt nanoparticles. Interestingly, there is a significant difference in n_{eff} for the two sizes of Pt DENs ($n_{eff} = 3.7$ and 3.5 for Pt_{147} and Pt_{55}, respectively) that cannot be assigned to mass transfer effects and that we therefore attribute to a particle size effect.

electrocatalysis | platinum nanoparticle

Here we report on the effect of mass transfer rate (k_t) on the oxygen reduction reaction (ORR) catalyzed by Pt dendrimer-encapsulated nanoparticles (DENs) comprised of 147 and 55 atoms (Pt_{147} and Pt_{55}, respectively). The experiments were carried out in the dual-electrode microelectrochemical device shown in Fig. 1 (1). This configuration enables the study of the ORR under high k_t conditions with simultaneous detection of H_2O_2. This is important because the methods currently used to study ORR at high k_t, such as ultramicroelectrodes (UMEs) (2), nanoelectrodes (3), and microjet electrodes (4) do not incorporate H_2O_2 detection. Accordingly, ORR data is generally interpreted based on steady-state, mass-transfer-limited currents alone. Using the microelectrochemical device, two principal effects are evident as k_t is increased. First, the ORR current becomes significantly smaller than predicted by the Levich equation (5). Second, the effective number of electrons involved in the ORR, n_{eff}, remains constant over the entire k_t range, for both Pt_{147} and Pt_{55}. We draw three conclusions from these observations: (*i*) The decrease in ORR current at high k_t is caused by kinetic effects; (*ii*) increasing k_t does not affect the mechanism of the ORR catalyzed by Pt DENs; and (*iii*) there is a difference in n_{eff} between Pt_{147} and Pt_{55} that cannot be attributed to mass-transfer effects.

The electrochemical ORR has been the subject of extensive research and has been reviewed on several occasions (6–10). The generally accepted mechanism for the ORR at a metallic surface is a multielectron reaction with intermediates as shown in Scheme 1 (2, 7, 9, 11). Specifically, at the electrode surface, O_2 can be reduced directly to H_2O or H_2O_2 in 4- or 2-electron processes, respectively. Subsequently, electrogenerated H_2O_2 can disproportionate into H_2O and O_2, or by addition of two electrons, form H_2O. According to Scheme 1, the yield of H_2O_2, quantified by n_{eff}, is determined by the relative rates of steps c, d, and e, as well as the rate of mass transfer of H_2O_2 away from the electrode surface (2).

The development of O_2/H_2 polymer electrolyte membrane fuel cells (PE-MFCs) as sustainable energy sources (12, 13) has led to increased interest in developing efficient, non-Pt catalysts for the ORR (14–18). In spite of this, Pt is still considered to be the most effective catalyst for the ORR, even though it is not optimal for this application due to its high overpotential and its low Earth abundance. In the absence of viable alternatives, interest has been focused on reducing the amount of Pt required for fuel cell applications. There are two ways to do this: dilute it with a second metal or decrease the size or total number of Pt monometallic catalyst particles. However, a decrease in Pt surface coverage (or, correspondingly, an increase in k_t) has been associated with slower ORR kinetics (19, 20) and an increase in the amount of H_2O_2 produced (21–23). The presence of H_2O_2 is a major concern for fuel cell applications due to its corrosive nature and because it lowers the maximum attainable voltage (24, 25).

A number of studies have been reported that focus on the role of mass transfer in ORR efficiency. The analytical tools used for this purpose include the rotating disk and rotating ring-disk electrodes (RDE and RRDE) (21, 26–28), UMEs (2, 29), nanoelectrodes (3), microjet electrodes (4), and microfluidic thin-layer cells (22, 23). In most of these studies, k_t is increased by decreasing the surface coverage of the catalyst (21–23, 27, 28). For example, Behm and coworkers studied the ORR using two-dimensional arrays of 100-nm Pt islands immobilized on glassy carbon (GC) electrodes (22, 23). The key finding was that the amount of electrogenerated H_2O_2 increased with decreasing catalyst coverage. A "desorption + readsorption + reaction" mechanism was proposed to explain this effect (26, 30). Under this assumption, more H_2O_2 is obtained at high k_t (low catalyst loading or high flow rates), due to lower probability for H_2O_2 readsorption and further reaction on different Pt sites (Scheme 1) (26, 30). Kucernak and coworkers studied the effect of high k_t conditions (up to 2 cm s^{-1}) on the ORR catalyzed by single, submicron Pt particles affixed to the ends of nanoelectrodes (3). It was found that the steady-state mass-transfer-limited current for the ORR decreased with increasing k_t. This was attributed to a shift in n_{eff} from 4 at $k_t = 0.01$ cm s^{-1} to 3.5 at $k_t = 2$ cm s^{-1} (3). However, because a collector electrode was not present, it was not possible to correlate these results to the presence of H_2O_2.

Here we study the effect of k_t on the ORR using Pt DENs having diameters of 1–2 nm and low (<0.3 nm) size polydispersity. In the microelectrochemical device shown in Fig. 1, Pt_{147} or

Author contributions: I.D. and R.M.C. designed research; I.D. performed research; I.D. analyzed data; and I.D. and R.M.C. wrote the paper.

The authors declare no conflict of interest.

This article is a PNAS Direct Submission.

[1]To whom correspondence should be addressed. E-mail: crooks@cm.utexas.edu.

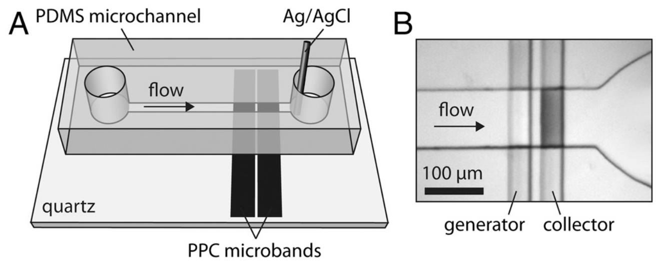

Fig. 1. (*A*) Schematic representation of the hybrid PDMS/quartz microelectrochemical device used for ORR studies. Solution is introduced to the microchannel using a syringe pump connected to the reservoir on the left. A combined reference/counter electrode is placed in the other reservoir so that it is in close proximity to PPC microband electrodes. Note that this drawing is not to scale. In the actual device, the length of the microband electrodes is typically 40 µm with a gap of 15 µm between them. (*B*) Optical micrograph of the PPC microbands and the microchannel after platinization of the collector electrode and electrochemical deposition of Pt DENs onto the generator electrode. The outlet reservoir is visible to the right of the electrodes.

Pt_{55} DENs are electrochemically immobilized onto a pyrolyzed photoresist carbon (PPC) generator electrode (1). This results in robust attachment of approximately 1 monolayer of Pt DENs onto the PPC surface (1). Importantly, a collector electrode is present downstream for amperometric detection of H_2O_2. By controlling the flow rate through the microchannel, it is possible to vary k_t between 0.02 and 0.12 $cm\,s^{-1}$. Indeed, such high mass transfer conditions are not achievable using the RRDE or UMEs with diameters larger than 2 µm. At low k_t (0.02 $cm\,s^{-1}$), which is similar to that achieved at the upper end of k_t values accessible with the RRDE, n_{eff} is 3.7 for Pt_{147} and 3.4 for Pt_{55}, in agreement with our previous findings (31). As k_t increases, the mass-transfer-limited current for the ORR becomes significantly lower than the value predicted by the Levich equation for a 4-electron process for both Pt_{147} and Pt_{55}. However, the percentage of H_2O_2 detected remains constant, such that n_{eff} does not change over the entire k_t range employed. Interestingly, there is a significant difference in n_{eff} for the two sizes of Pt DENs (average $n_{eff} = 3.7$ and 3.5 for Pt_{147} and Pt_{55}, respectively) that cannot be assigned to mass transfer effects.

The results reported here are significant for several reasons. First, we show that simultaneous measurement of the H_2O_2 current is vital for correct interpretation of ORR data. Second, while others have previously shown that the ORR catalyzed by large Pt nanoparticles is affected by changes in k_t (22, 23) we show here that this does not apply for smaller Pt materials. Finally, we show that the size of very small Pt nanoparticles (diameters <2 nm) has an effect on the mechanism of the ORR, and hence its product distribution. These observations are relevant to the development of efficient Pt electrocatalysts for the ORR.

Results and Discussion

Evaluation of ORR Activity for Pt_{147} and Pt_{55} at Low Mass Transfer Rates. The ORR activity of Pt_{147} and Pt_{55} DENs was evaluated using the poly(dimethylsiloxane) (PDMS)/quartz hybrid microelectrochemical device shown in Fig. 1 and discussed in detail elsewhere (1). Following platinization of the collector (Fig. 1*B*) and immobilization of Pt DENs on the generator (1), the ORR measurements were carried out in air-saturated 0.10 M $HClO_4$ electrolyte solution. To evaluate the ORR kinetics at low k_t, solution was flowed through the device at 0.05 µL min^{-1} (0.04 $cm\,s^{-1}$), corresponding to a k_t value of 0.02 $cm\,s^{-1}$. This is on the same order as that achieved using an RRDE.

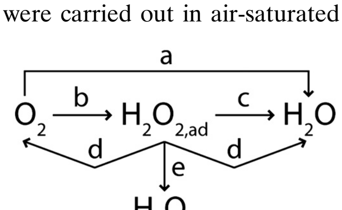

Scheme 1.

We previously used the RDE to evaluate the ORR characteristics of Pt DENs having different sizes (31). The results showed that the steady-state limiting current for Pt_{147} was higher than for Pt_{55}, an effect that was tentatively assigned to H_2O_2 becoming a significant product of the ORR for the smaller catalytic particles (31). We pointed out that if this were correct, it was a rare case of a very slight change in particle size resulting in a shift in product distribution. Fig. 2 shows generation-collection linear scan voltammograms (LSVs) for the ORR obtained using the microelectrochemical device for Pt_{147} (blue lines) and Pt_{55} (red lines) DENs at $k_t = 0.02$ $cm\,s^{-1}$. The potential of the generator electrode was swept from +0.80 to −0.10 V (vs. Ag/AgCl) at 50 $mV\,s^{-1}$. The potential of the collector electrode was held at +1.10 V, where we observed reliable and stable mass-transfer-limited currents for H_2O_2 oxidation (1). The onset of catalytic current is at $\sim +0.60$ V, and a steady-state, mass-transfer-limited current is apparent over the range 0.00 to −0.10 V. There is a slight decrease in the ORR current at potentials more negative than 0 V due to hydrogen adsorption onto the catalyst (32). In addition, the adsorption of hydrogen is accompanied by an increase in hydrogen peroxide formation (manifested as an increase in the collector electrode current), an effect previously observed by others (32). To minimize artifacts arising from hydrogen adsorption, generator-collector current pairs were measured at the potential where the ORR current reached its maximum value.

Importantly, the ORR limiting current for Pt_{147} DENs (55 nA) is noticeably higher than for Pt_{55} DENs (37 nA), although the LSVs have the same general shape. The downstream collector electrode makes it possible to determine the amount of H_2O_2 produced during ORR, at the same time the mass-transfer-limited currents are measured at the generator. The LSVs in Fig. 2 show that the amount of H_2O_2 oxidized at the collector electrode is higher for Pt_{55} DENs. As we hypothesized in our earlier publication, this indicates that the peroxide pathways play a more important role in the ORR catalyzed by smaller nanoparticles (31).

The value of n_{eff} was determined using the ratio of the steady-state mass-transfer-limited current for the ORR (i_{gen}) and the oxidation current for H_2O_2 (i_{col}); that is, $n_{eff} = 4 - [(2i_{col})/(\eta i_{gen})]$, where η represents the collection efficiency of the device (details on how η is calculated are provided in *Materials and Methods*) (33). In Fig. 2, i_{col} has been background subtracted against the current value obtained by holding the collector electrode at a potential (1.10 V), where the ORR does not proceed. The measured η at 0.05 µL min^{-1} was 40.0%. Note that the collector cur-

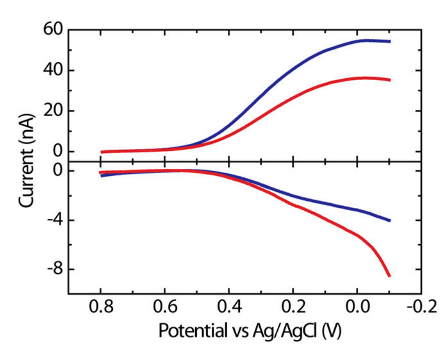

Fig. 2. Generation (upper curves) and collection (lower curves) LSVs obtained using Pt_{147} (blue lines) and Pt_{55} (red lines) DENs in air-saturated, aqueous 0.10 M $HClO_4$. The potential of the generator electrode was scanned from +0.80 to −0.10 V (vs. Ag/AgCl) while holding the potential of the platinized collector at +1.10 V. The flow rate was 0.05 µL min^{-1} corresponding to $k_t = 0.02$ $cm\,s^{-1}$, and η was 40.0%. The scan rate was 50 $mV\,s^{-1}$.

rent does not exhibit a clear, steady-state plateau (*vide supra*), and, as such, i_{col} was measured at the potential where i_{gen} attained its maximum value (0 V). The calculated values of n_{eff} are 3.7 ± 0.1 and 3.4 ± 0.1 (average of three independent measurements), for Pt_{147} and Pt_{55}, respectively. Using these values for n_{eff}, i_{gen} can be estimated using the Levich equation (Eq. **1**) (5), as follows:

$$i_{gen} = 0.925 n_{eff} F c_{O_2} D_{O_2}^{2/3} V_f^{1/3} \left(\frac{h^2 d}{4}\right)^{-1/3} w x_e^{2/3}. \quad [1]$$

Here, F is the Faraday constant, c_{O2} and D_{O2} are the bulk concentration and diffusion coefficient, respectively, of O_2 [$c_{O2} =$ 0.20 mM, (34) $D_{O2} = 1.67 \times 10^{-5}$ cm^2 s^{-1}] (35), V_f is the volume flow rate (0.05 μL min^{-1}), x_e and w are the length (40 μm) and the width (100 μm) of the electrode, respectively, d is the width of the microchannel (100 μm), and h is the height of the microchannel (20 μm). Using the previously determined n_{eff} values, i_{gen} is calculated to be 55 nA for Pt_{147} and 50 nA for Pt_{55}. For Pt_{147}, the calculated value is in excellent agreement with the measured i_{gen} of 55 nA. However, for Pt_{55}, the calculated value is substantially higher than the experimentally determined i_{gen} (37 nA). Although we do not understand this result, such inconsistencies are common in the ORR RRDE literature (36, 37). It is possible that the relatively high scan rate employed (50 mV s^{-1}) also contributes to this effect.

ORR Measurements at High Mass Transfer Rates. To learn more about the effect of the mass transfer rate of O_2 on n_{eff}, we acquired ORR generation collection LSVs while flowing air-saturated 0.10 M $HClO_4$ through the microchannel at flow rates ranging from 0.05 to 10 μL min^{-1} (0.04 to 8.3 cm s^{-1}). This corresponds to k_t values from 0.02 to 0.12 cm s^{-1}. This range is considerably higher than that accessible with the RRDE. Indeed, to achieve the upper limit of $k_t = 0.12$ cm s^{-1}, a RRDE would have to be rotated at 150,000 rpm, which is well above the typical maximum rotation rate of 7,000 rpm. Fig. 3*A* shows a plot of i_{gen} and simultaneously measured i_{col} values obtained for Pt_{147} (blue dots) and Pt_{55} (red dots) as a function of flow. Values for i_{gen} and i_{col} were obtained from both low-to-high and high-to-low flow rates, and were found to be independent of this parameter. This confirms that the Pt coverage is constant throughout the experiments (that is, that the Pt DENs remain attached to the electrode surface). In Fig. 3*A*, i_{col} was normalized with respect to η for each flow rate. Recall that $i_{gen} - i_{col}$ current pairs were measured at the potential where i_{gen} reached its maximum value and i_{col} values were background subtracted (*vide supra*). Fig. 3*A* shows that, for both Pt_{147} and Pt_{55} DENs, as k_t increases, i_{gen} increases and begins to level off at flow rates higher than 2 μL min^{-1}. The same pattern is observed for i_{col}. Furthermore, across the entire flow-rate range, the ORR limiting current for Pt_{147} remains higher than that for Pt_{55}.

It is interesting to compare the experimental values of i_{gen} with the theoretical values predicted by the Levich equation (Eq. **1**) for 4- and 2-electron ORR processes. In Fig. 3*B*, the i_{gen} values from Fig. 3*A* are plotted vs. $V_f^{1/3}$ and k_t. The current for 4- and 2-electron ORR processes are plotted on the same graph (dashed lines). For Pt_{147}, Fig. 3*B* indicates that as k_t increases, i_{gen} appears to drift from the 4-electron to the 2-electron ORR pathway (Scheme 1). Interestingly, at V_f higher than 1 μL min^{-1}, the measured i_{gen} for Pt_{55} is smaller than the value predicted by Eq. **1** for a 2-electron process, an observation that will be discussed later. Importantly, for both Pt_{147} and Pt_{55} DENs, the plot of i_{gen} vs. $V_f^{1/3}$ is not linear. A similar trend in the ORR limiting current was observed during Pt-catalyzed ORR studies using UMEs (2) and nanoelectrodes (3), and for Cu using hydrodynamic electrodes (4). These results were interpreted in terms of O_2 reduction not following a simple 4- or 2-electron transfer process, but instead undergoing a transition from 4 electrons at the lowest k_t values towards 2 electrons as the mass transfer rate increased. It is important to note that in these earlier reports a collector electrode was not used, and therefore the amount of H_2O_2 generator could not be measured directly and then correlated to the ORR current. Because we (1) and others (36, 37) have noted that the mass-transfer-limited current for the ORR is often unreliable for the determination of n_{eff}, an accurate calculation requires the ratio of i_{col} to i_{gen}. Here, the concomitant measurement of H_2O_2 oxidation current allows the calculation of n_{eff} at each k_t value. Fig. 4 shows a plot of n_{eff} vs. V_f and k_t, calculated for data presented in Fig. 3*A*. At all but the lowest flow rates, the value of n_{eff} (that is, the percentage of H_2O_2 collected during ORR) is nearly constant. Consequently, although the magnitude of i_{gen} suggests a shift in the mechanism of ORR with the change in mass transfer rate, n_{eff} remains constant over the entire k_t range. The average n_{eff} is 3.7 and 3.5 for Pt_{147} and Pt_{55}, respectively, similar to the values calculated at $k_t = 0.02$ cm s^{-1} (3.7 for Pt_{147} and 3.4 for Pt_{55}). We attribute the shift in i_{gen} observed here, and previously by others (2–4) to kinetic effects: As k_t increases, some O_2 molecules flow past the generator electrode faster than they can be reduced. This results in a decrease in i_{gen} from its theoretical mass-transfer-limited value. However, the mechanism of ORR remains unaffected. Although we do not currently have a definitive explanation for the difference in n_{eff} between Pt DENs of different sizes, it is possible that the decrease in particle size leads to a different O_2 binding mechanism onto the Pt surface, which ultimately affects the ORR pathway. For small Pt NPs, molecular O_2 can bind to corner and edge sites in the so-called single-bond binding geometry, in which one oxygen atom is against the metal surface

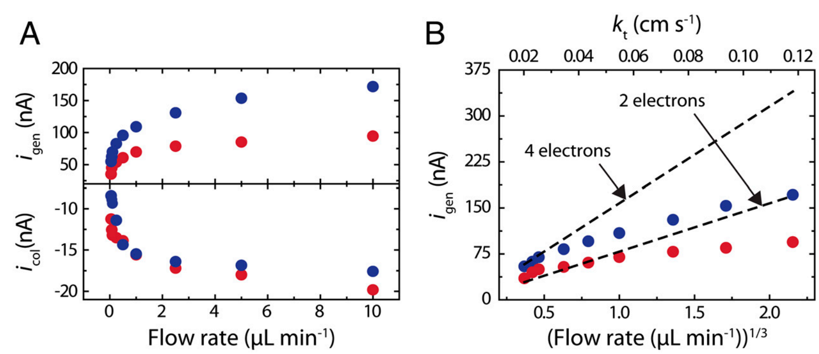

Fig. 3. (*A*) Plot of i_{gen} (ORR mass-transfer-limited current) and simultaneously acquired i_{col} (H_2O_2 oxidation current) for Pt_{147} (blue circles) and Pt_{55} (red circles) measured while flowing air-saturated, aqueous 0.10 M $HClO_4$ through the microchannel at flow rates ranging from 0.05 to 10 μL min^{-1} (k_t from 0.02 to 0.12 cm s^{-1}). Note that i_{col} was normalized with respect to η (η values for 0.05, 0.075, 0.1, 0.25, 0.5, 1, 2.5, 5, and 10 μL min^{-1} flow rates were 40.0, 37.2, 36.3, 34.7, 34.2, 34.0, 33.5, 33.3 and 32.7%, respectively). (*B*) Plot of i_{gen} from *A* vs. $V_f^{1/3}$ and k_t, for Pt_{147} (blue circles) and Pt_{55} (red circles). The dashed black lines were calculated using the Levich equation (Eq. **1**) for a 4-electron (upper line) and a 2-electron (lower line) process.

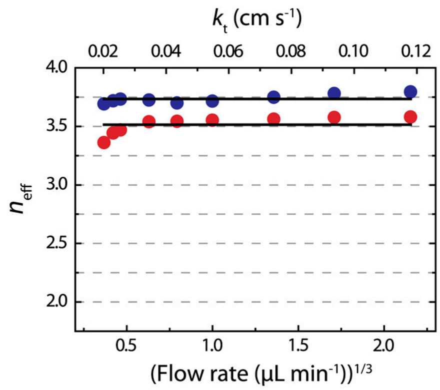

Fig. 4. The value of n_{eff} calculated from the experimental results in Fig. 3*A* for Pt_{147} (blue circles) and Pt_{55} (red circles) vs. $V_f^{1/3}$ and k_t. The black lines represent the average values of n_{eff} across the entire mass transfer range shown.

and the second is exposed to the solvent. Such single-bond binding can lead to the formation of OOH groups, and ultimately, H_2O_2. Experimental and theoretical work is currently underway to fully understand this effect.

Conclusions

Using a dual-electrode microelectrochemical device we investigated the effect of mass transfer on the ORR catalyzed by Pt_{147} and Pt_{55} DENs. At low values of k_t (0.02 $cm\,s^{-1}$), n_{eff} was 3.7 for Pt_{147} and 3.4 for Pt_{55}, in agreement with previous findings obtained using a RDE (31). As k_t was increased from 0.02 to 0.12 $cm\,s^{-1}$, the measured ORR mass-transfer-limited current for both Pt_{147} and Pt_{55} was smaller than the value predicted by the Levich equation, similar to results obtained by others (2–4). Previously, this was interpreted as a transition of the ORR from four electrons at the lowest k_t values towards two electrons as the mass transfer rate increased. Here, we observed that the percentage of H_2O_2 produced was unaffected by k_t, and n_{eff} was nearly constant across the entire k_t range. Hence, the concomitant measurement of H_2O_2 allows us to conclude that the decrease in the expected mass-transfer-limited current for ORR at high k_t is in fact due to kinetic effects, rather than a change in the ORR mechanism.

Importantly, we also observed an unambiguous nanoparticle size effect on the mechanism of ORR, with an average n_{eff} higher for Pt_{147} (3.7) than for Pt_{55} (3.5). It is certainly surprising that a change in particle size of just 100 atoms is able to shift the reaction mechanism. Accordingly, we are investigating this effect in more detail, as it may have an important role to play in ORR electrocatalysis specifically and electrocatalysis generally. The results of these studies will be reported in due course.

Materials and Methods

Chemicals. PDMS channels were prepared using a Sylgard 184 elastomer kit obtained from K. R. Anderson, Inc. Quartz microscope slides (25 mm × 75 mm, 1 mm thick) were purchased from Technical Glass Products. Positive-tone photoresist (AZ 1518) and developer (AZ 400K) were purchased from Capitol Scientific, Inc. Sixth-generation poly(amidoamine) dendrimers terminated with hydroxyl groups (G6-OH) were purchased as a 5% (wt/wt) solution in methanol (Dendritech, Inc.). Prior to use, the methanol was removed under vacuum and the dendrimer was reconstituted in water at a concentration of 100 μM. K_2PtCl_4 (99.99%), $NaBH_4$ (99.99%), and $LiClO_4$ (99.99%) were purchased from Sigma-Aldrich, Inc.; $HClO_4$ (Ultrex II) was from J. T. Baker and ferrocenemethanol (FcMeOH, 97%) was from Acros Organics. These reagents were used without further purification. Deionized water having a resistivity of 18.2 MΩ cm was used for all experiments (Milli-Q gradient system, Millipore).

Preparation of Microelectrochemical Devices. The procedure for fabricating PPC microband electrodes is described in detail elsewhere (1). Briefly, PPC microbands, 40 μm wide and separated by a 15 μm gap, were fabricated by slow pyrolysis of patterned AZ 1518 photoresist at 1,000 °C under a forming gas of 5% H_2 and 95% N_2 (1). The thickness of the resulting PPC features, measured using profilometry, was 300 nm. PDMS microfluidic channels, 6 mm long, 100 μm wide and 20 μm high, were prepared using a previously described replica micromolding method (1, 38). Two reservoirs (1.0 mm diameter) were punched at the ends of each channel to accommodate introduction of solution. The PDMS layer and quartz substrate were exposed to an air plasma (60 W, model PDC-32G, Harrick Scientific) for 45 s, joined together under an optical microscope, and then placed over a hot plate at 80 °C for 5 min. A syringe pump (Pump 11, Pico Plus Elite, Harvard Apparatus), connected to the inlet (left side) reservoir using Teflon tubing, was used to push solution through the microelectrochemical device.

Preparation of Pt DENs. Pt DENs comprised of 147 and 55 atoms were prepared according to our previously published procedure (31, 39). A 0.10 mM aqueous solution of G6-OH was mixed with sufficient aqueous 0.10 M K_2PtCl_4 such that the final Pt^{2+}-to-dendrimer ratios were 147 : 1 or 55 : 1. After stirring for three days (40), a 10-fold molar excess of aqueous 1.00 M $NaBH_4$ was added to reduce Pt^{2+}. This solution was kept capped for 24 h to maximize reduction of Pt^{2+} (40). Note that we have previously shown that reduction of the Pt^{2+}/G6-OH precursor by BH_4^- does not yield fully reduced Pt DENs (40, 41). However, electrochemical cycling does result in complete reduction (*vide infra*) (40, 41). The average diameters and size distributions of the Pt DENs were 1.7 nm and 1.4 nm for Pt_{147} and Pt_{55}, respectively (31). After synthesis, the quality of the Pt DENs was verified by UV-vis absorption spectroscopy (31, 42). Before using for electrochemical experiments, Pt DENs were dialyzed for 24 h in 4.0 L of Millipore water (Milli-Q Gradient PF-06073) to remove salts and other impurities. After dialysis, but prior to immobilization onto PPC electrodes, the DEN solution was mixed with sufficient $LiClO_4$ to yield a 0.10 M solution.

Electrochemistry. The microelectrochemical device was configured in a three-electrode arrangement, comprising the two PPC microbands as working electrodes. A Ag/AgCl reference electrode, which also acted as a counter electrode was positioned in the outlet (right-hand side) reservoir (Scheme 1). All potentials are referenced to Ag/AgCl (3.4 M KCl, model 66-EE009 "no-leak" Ag/AgCl, Dionex). LSV with two working electrodes was carried out using a computer-based bipotentiostat (Model CHI760B potentiostat, CH Instruments). All electrochemical experiments were performed at 22 ± 1 °C.

Prior to the immobilization of Pt DENs on the generator, Pt was electrodeposited onto the PPC collector electrode to increase its sensitivity for amperometric H_2O_2 detection (Fig. 1*B*) (1). After platinization, LSVs were acquired at the PPC generator electrode in the ORR region of interest (+0.80 to −0.10 V vs. Ag/AgCl) using aqueous 0.10 M $HClO_4$, to check that the generator electrode had not been contaminated with Pt during the platinization step. Pt DENs were then immobilized on the PPC generator using a previously reported procedure (1, 31, 39). Briefly, a 10.0 μM Pt DEN solution containing 0.10 M $LiClO_4$ was flowed through the microchannel at 0.05 $\mu L\,min^{-1}$ while the electrode potential was swept three times between +0.10 and +1.00 V (vs. Ag/AgCl) at 10 $mV\,s^{-1}$. We previously showed that this results in robust attachment of approximately 1 monolayer of Pt DENs onto both GC and PPC surfaces (1, 31). Before acquiring ORR generation collection LSVs, the DEN-modified electrodes were scanned 20 times at 100 $mV\,s^{-1}$ between +1.25 V and −0.20 V (vs. Ag/AgCl) in air-saturated 0.10 M $HClO_4$ solution. As we have shown previously, these conditioning scans (43) are commonplace and required to achieve stable and reproducible LSVs (39).

Upon completion of the ORR measurements, η was determined for each microelectrochemical device using the following method. Generation collection LSVs were recorded while pumping an aqueous solution containing 0.10 mM FcMeOH and 0.10 M KNO_3 through the microchannel at flow rates ranging from 0.05 to 10 $\mu L\,min^{-1}$ (0.04 to 8.3 $cm\,s^{-1}$). At each flow rate, the values of η were calculated as the ratio of the steady-state mass-transfer-limited currents at the collector and generator electrodes, for the electrolysis of FcMeOH. The calculated values of η ranged from 32.7–40.0%.

ACKNOWLEDGMENTS. We thank Prof. Julie MacPherson (Warwick University) for enlightening discussions. We gratefully acknowledge financial support from the US Department of Energy, Office of Basic Energy Sciences (Grant No. DE-FG02-09ER16090). Sustained support from the Robert A. Welch Foundation (Grant F-0032) is also acknowledged.

1. Dumitrescu I, Yancey DF, Crooks RM (2012) Dual-electrode microfluidic cell for characterizing electrocatalysts. *Lab Chip* 12:986–993.
2. Pletcher D, Sotiropoulos SA (1993) Study of cathodic oxygen reduction at platinum using microelectrodes. *J Electroanal Chem* 356:109–119.
3. Chen S, Kucernak A (2004) Electrocatalysis under conditions of high mass transport rate: Oxygen reduction on single submicrometer-sized Pt particles supported on carbon. *J Phys Chem B* 108:3262–3276.
4. Colley AL, Macpherson JV, Unwin PR (2008) Effect of high rates of mass transport on oxygen reduction at copper electrodes: Implications for aluminium corrosion. *Electrochem Commun* 10:1334–1336.
5. Levich VG (1962) *Physicochemical Hydrodynamics* (Prentice Hall, Englewood Cliffs, NJ), 2nd Ed.
6. Yeager E (1984) Electrocatalysts for O_2 reduction. *Electrochim Acta* 29:1527–1537.
7. Yeager E (1986) Dioxygen electrocatalysis: Mechanisms in relation to catalyst structure. *J Mol Catal* 38:5–25.
8. Kinoshita K (1992) *Electrochemical Oxygen Technology* (Wiley, New York).
9. William M, Jai P (2003) *Fundamental Understanding of Electrode Processes in Memory of Professor Ernest B. Yeager* (The Electrochemical Society, Pennington, NJ).
10. Savéant JM (2008) Molecular catalysis of electrochemical reactions. Mechanistic aspects. *Chem Rev* 108:2348–2378.
11. Wroblowa HS, Yen Chi P, Razumney G (1976) Electroreduction of oxygen: A new mechanistic criterion. *J Electroanal Chem Interfac Electrochem* 69:195–201.
12. Costamagna P, Srinivasan S (2001) Quantum jumps in the PEMFC science and technology from the 1960s to the year 2000: Part I. Fundamental scientific aspects. *J Power Sources* 102:242–252.
13. O'Hayre R, Suk-Won C, Colella W, Prinz FB (2006) *Fuel Cell Fundamentals* (Wiley, Hoboken, NJ).
14. Marković NM, Schmidt TJ, Stamenković V, Ross PN (2001) Oxygen reduction reaction on Pt and Pt bimetallic surfaces: A selective review. *Fuel Cells* 1:105–116.
15. Spendelow JS, Wieckowski A (2007) Electrocatalysis of oxygen reduction and small alcohol oxidation in alkaline media. *Phys Chem Chem Phys* 9:2654–2675.
16. Manthiram A, Vadivel Murugan A, Sarkar A, Muraliganth T (2008) Nanostructured electrode materials for electrochemical energy storage and conversion. *Energy Environ Sci* 1:621–638.
17. Peng Z, Yang H (2009) Designer platinum nanoparticles: Control of shape, composition in alloy, nanostructure and electrocatalytic property. *Nano Today* 4:143–164.
18. Gewirth AA, Thorum MS (2010) Electroreduction of dioxygen for fuel-cell applications: Materials and challenges. *Inorg Chem* 49:3557–3566.
19. Gasteiger HA, Panels JE, Yan SG (2004) Dependence of PEM fuel cell performance on catalyst loading. *J Power Sources* 127:162–171.
20. Neyerlin KC, Gu W, Jorne J, Gasteiger HA (2007) Study of the exchange current density for the hydrogen oxidation and evolution reactions. *J Electrochem Soc* 154: B631–B635.
21. Inaba M, Yamada H, Tokunaga J, Tasaka A (2004) Effect of agglomeration of Pt/C catalyst on hydrogen peroxide formation. *Electrochem Solid-State Lett* 7:A474–A476.
22. Schneider A, et al. (2008) Transport effects in the oxygen reduction reaction on nanostructured, planar glassy carbon supported Pt/GC model electrodes. *Phys Chem Chem Phys* 10:1931–1943.
23. Seidel YE, et al. (2008) Mesoscopic mass transport effects in electrocatalytic processes. *Faraday Discuss* 140:167–184.
24. Borup R, et al. (2007) Scientific aspects of polymer electrolyte fuel cell durability and degradation. *Chem Rev* 107:3904–3951.
25. Sethuraman VA, Weidner JW, Haug AT, Pemberton M, Protsailo LV (2009) Importance of catalyst stability vis-à-vis hydrogen peroxide formation rates in PEM fuel cell electrodes. *Electrochim Acta* 54:5571–5582.
26. Ke K, Hatanaka T, Morimoto Y (2011) Reconsideration of the quantitative characterization of the reaction intermediate on electrocatalysts by a rotating ring-disk electrode: The intrinsic yield of H_2O_2 on Pt/C. *Electrochim Acta* 56:2098–2104.
27. Ruvinskiy P, Bonnefont A, Savinova E (2011) Further insight into the oxygen reduction reaction on Pt nanoparticles supported on spatially structured catalytic layers. *Electrocatal* 2:123–133.
28. Ruvinskiy PS, Bonnefont A, Pham-Huu C, Savinova ER (2011) Using ordered carbon nanomaterials for shedding light on the mechanism of the cathodic oxygen reduction reaction. *Langmuir* 27:9018–9027.
29. Birkin PR, Elliott JM, Watson YE (2000) Electrochemical reduction of oxygen on mesoporous platinum microelectrodes. *Chem Commun* 1693–1694.
30. Fuhrmann J, et al. (2011) The role of reactive reaction intermediates in two-step heterogeneous electrocatalytic reactions: A model study. *Fuel Cells* 11:501–510.
31. Ye H, Crooks JA, Crooks RM (2007) Effect of particle size on the kinetics of the electrocatalytic oxygen reduction reaction catalyzed by Pt dendrimer-encapsulated nanoparticles. *Langmuir* 23:11901–11906.
32. Stamenkovic VM, Markovic N, Ross PN, Jr (2001) Structure-relationships in electrocatalysis: Oxygen reduction and hydrogen oxidation reactions on Pt(111) and Pt(100) in solutions containing chloride ions. *J Electroanal Chem* 500:44–51.
33. Antoine O, Durand R (2000) RRDE study of oxygen reduction on Pt nanoparticles inside Nafion: H_2O_2 production in PEMFC cathode conditions. *J Appl Electrochem* 30:839–844.
34. Truesdale GA, Downing AL, Lowden GF (1955) The solubility of oxygen in pure water and sea-water. *J Appl Chem* 5:53–62.
35. Zagal J, Bindra P, Yeager E (1980) A mechanistic study of O_2 reduction on water soluble phthalocyanines adsorbed on graphite electrodes. *J Electrochem Soc* 127:1506–1517.
36. Luo J, Njoki PN, Lin Y, Wang L, Zhong CJ (2006) Activity-composition correlation of AuPt alloy nanoparticle catalysts in electrocatalytic reduction of oxygen. *Electrochem Commun* 8:581–587.
37. Chen W, Ny D, Chen S (2010) SnO2-Au hybrid nanoparticles as effective catalysts for oxygen electroreduction in alkaline media. *J Power Sources* 195:412–418.
38. Hlushkou D, Perdue RK, Dhopeshwarkar R, Crooks RM, Tallarek U (2009) Electric field gradient focusing in microchannels with embedded bipolar electrode. *Lab Chip* 9:1903–1913.
39. Ye H, Crooks RM (2005) Electrocatalytic O_2 reduction at glassy carbon electrodes modified with dendrimer-encapsulated Pt nanoparticles. *J Am Chem Soc* 127:4930–4934.
40. Knecht MR, et al. (2008) Synthesis and characterization of Pt dendrimer-encapsulated nanoparticles: Effect of the template on nanoparticle formation. *Chem Mater* 20:5218–5228.
41. Myers VS, Frenkel AI, Crooks RM (2012) In situ structural characterization of platinum dendrimer-encapsulated oxygen reduction electrocatalysts. *Langmuir* 28:1596–1603.
42. Ye H, Scott RWJ, Crooks RM (2004) Synthesis, characterization, and surface immobilization of platinum and palladium nanoparticles encapsulated within amine-terminated poly(amidoamine) dendrimers. *Langmuir* 20:2915–2920.
43. Garsany Y, Baturina OA, Swider-Lyons KE, Kocha SS (2010) Experimental methods for quantifying the activity of platinum electrocatalysts for the oxygen reduction reaction. *Anal Chem* 82:6321–6328.